Cellulose (2023) 30:11323–11340
https://doi.org/10.1007/s10570-023-05584-z

ORIGINAL RESEARCH

Patterns in interactions of variably acetylated xylans with hydrophobic cellulose surfaces

Madhulika Gupta · Paul Dupree · Loukas Petridis · Jeremy C. Smith

Received: 27 February 2023 / Accepted: 22 October 2023 / Published online: 6 November 2023
© The Author(s), under exclusive licence to Springer Nature B.V. 2023

Abstract The recalcitrance of plant cell wall lignocellulosic biomass to deconstruction is a major hurdle to sustainable biofuel/bioproduct economy. A multitude of interactions stabilize lignocellulosic biomass structure. Among these, tight packing of hemicellulose-cellulose is partly responsible for biomass recalcitrance. Here, unrestrained molecular dynamics simulations are employed to understand the influence of the nature and pattern of naturally-occuring acetyl decorations of the xylan backbone on interactions with the (100) hydrophobic cellulose surface. Periodically O2-acetylated xylan (2AcX) assume twofold helical screw conformations that are stabilized by a combination of multiple hydrophobic contacts and hydrogen bonds with the hydrophobic cellulose surface. In contrast, acetylation at the O3 position in xylan obstructs interactions, thereby adopting threefold helical screw conformations that potentially preferably interact with lignin rather than cellulose. Fully acetylated xylan desorbs from the surface implying a minimum number of unsubstituted residues on the xylan backbone is required for interaction with the surface. The substituted residues must form ~ 20% fewer contacts than the unsubstituted residues to sustain stable twofold helical screw xylan conformations on the cellulose surface. Thus, specific roles of macromolecular conformations of cellulose and hemicellulose in influencing the supramolecular interactions and function of plant cell walls have been determined.

Keywords Acetylation · Plant cell wall architecture · Substitution pattern · Threefold helical screw xylan conformations · Twofold helical screw · Cellulose

M. Gupta (✉)
Computational Biophysics Lab, Department of Chemistry and Chemical Biology, Indian Institute of Technology (Indian School of Mines), Dhanbad, Jharkhand 826004, India
e-mail: madhulikagupta@iitism.ac.in

P. Dupree
Department of Biochemistry and Leverhulme Centre for Natural Material Innovation, University of Cambridge, Cambridge CB2 1QW, UK

L. Petridis · J. C. Smith (✉)
Oak Ridge National Lab, UT/ORNL Center for Molecular Biophysics, Oak Ridge, TN 37831, USA
e-mail: smithjc@ornl.gov

L. Petridis · J. C. Smith
Department of Biochemistry and Cellular and Molecular Biology, University of Tennessee, Knoxville, TN 37996, USA

Introduction

Plant biomass is a heterogeneous composite material comprising mostly cellulose and hemicellulose linked tightly with lignins (Chundawat et al. 2011). The complex interactions among these components play a key role in the mechanical strength and rigidity of plant cell walls. The structural heterogeneity involved

limits our understanding of cell-wall architecture, thereby hindering the full exploitation of this abundant resource for the sustainable production of biofuels and bio-based advanced materials (Köhnke et al. 2011). In the current era of climate change, with ever increasing CO_2 emissions and depleting fossil fuels, it is important to develop lignocellulosic biomass as an energy source and explore it to its full potential. A detailed understanding of the structure–function relationships in plant cell walls is central to developing cost-effective technology to solubilize and fractionate biomass into cellulose, hemicellulose, and lignin to process them individually for further use. Thus, it is of utmost importance to obtain a deeper insight into the interactions that stabilize cell wall structure (Celińska et al. 2021).

Cellulose microfibrils comprise β-(1,4)-linked D-glucosyl chains that have highly ordered structures and form bundles with increased disorder towards the surface leading to twisting of the microfibrillar structure (Bootten et al. 2004; Cosgrove and Jarvis 2012). The microfibrils have surfaces parallel to different crystallographic planes and these surfaces are designated based on the Miller indices used to define these planes. The exact surfaces exposed in these fibrils for interactions with hemicellulose is still a matter of debate but for convention, (110), (1–10) or (010) planes are considered as "hydrophilic" surfaces, while (100) or (200) planes that are parallel to each other are considered as "hydrophobic" surface. The most common hemicellulose, xylan, is made up of β-(1,4)-linked D-xylosyl units and is the major component in hardwood and grasses, thus categorizing it as one of the abundant sources of renewable energy (Wierzbicki et al. 2019; Tryfona et al. 2023). The xylan backbone is further substituted by various side chains like glucuronic acid (GlcA), 4-O-methylglucuronic acid (MeGlcA), arabinose (Ara) or acetyl (Ac) groups to mediate the function of cell walls (Ebringerova and Heinze 2000; Scheller and Ulvskov 2010). Glucuronidation plays an important role in regulating the interconnectivity of xylan and lignin. In contrast, the presence of Ac groups plays a crucial role in dictating the interchain attractions, the solubility of xylan chain and the resistance to enzymatic and microbial degradation (Pawar et al. 2013).

Ac groups tailor the hydrophilicity of the xylan backbone and may modulate interactions with hydrophobic and hydrophilic cellulose surfaces. The degree of acetylation of xylan varies depending upon the plant taxonomy. Acetylation can be as high as 0.7 in the case of hardwood xylans or as low as 0.06 in Poplar (Pawar et al. 2013; Johnson et al. 2017). Any decrease in the acetyl content in xylan backbone is observed to decrease the mechanical strength of plant cell walls and instigate structural abnormalities. Acetylation also plays a role in enhancing thermal stability of xylan walls and enhances the glass transition temperature (de Carvalho et al. 2019). Subsequently, the presence of excessive decorations on the xylan chain can decrease the extent of adsorption with the cellulose surface. Such effects are more pronounced for Ara rather than Ac substitutions (Kabel et al. 2007; Bosmans et al. 2014).

The nature and position of substitutions on the hemicellulose further play a key role in influencing the interactions with cellulose surfaces as well as the lignin by adopting specific conformations (Kang et al. 2019). In solution, in the absence of cellulose, xylan forms a threefold helical screw conformation while when interacting with cellulose, periodically substituted xylan adopts a twofold helical screw (Simmons et al. 2016). The energetic barrier between twofold and threefold helical conformations is rather low, allowing rapid interconversion between the two (Berglund et al. 2016). However, twofold conformations dominate on the cellulose surface if they are stabilized by specific interactions between the xylan and the cellulose (Teleman et al. 2002; Busse-Wicher et al. 2014, 2016; Simmons et al. 2016; Martínez-Abad et al. 2017; Gupta et al. 2021). The cellulose, on the other hand, maintains a rigid twofold helical conformation due to favourable chain packing owing to dispersion interactions. In addition, the presence of an exocyclic CH_2OH group and intra-molecular hydrogen bonds facilitate this chain packing in cellulose (Pereira et al. 2017; Ling et al. 2020).

The topography of the cellulose surface also dictates the orientation of the xylan conformations. For example, the roughness of the hydrophilic cellulose face does not support the formation of the twofold helical screw (Zhao et al. 2014). In contrast, the hydrophobic surface has a higher affinity for xylan than the hydrophilic surface (Cosgrove 2014). Even at high temperatures, glucuronoarabinoxylan diffuses from the hydrophilic to the hydrophobic surfaces (Pereira et al. 2017). The hydrophilic surface stabilizes the xylan backbone by hydrogen bonding

interactions while the hydrophobic surface uses hydrophobic interactions to stabilize xylan conformations. Indeed, the importance of hydrophobic effects in stabilizing both hemicellulose and DNA interactions with cellulose and their role in cellulose dissolution has been a recent topic of study (Lindman et al. 2021; Wohlert et al. 2022).

Several studies show that the presence of an alternate pattern of acetylation on the xylan backbone is a prerequisite for interactions with the hydrophilic cellulose surface (Busse-Wicher et al. 2014, 2016; Falcoz-Vigne et al. 2017; Grantham et al. 2017) but may not be important for the hydrophobic surface (Busse-Wicher et al. 2014, 2016). Molecular dynamics (MD) simulations show that the presence of an even pattern of Ara and MeGlcA residues on xylan backbone leads to favourable adsorption of the xylan chain on both hydrophobic and hydrophilic surfaces (Martínez-Abad et al. 2017). The presence of Ac residues in an ordered even pattern has also been shown to fit perfectly to provide a surface for interactions with the hydrophilic surface, thereby lending structural rigidity to plant cell walls (Gupta et al. 2021). However, similar data for acetylated xylans on the hydrophobic surface are not available.

One of the well-studied relevant systems is the *Arabidopsis* stem whose molecular arrangement has been studied extensively using mass spectrometry and nuclear magnetic resonance (NMR) (Busse-Wicher et al. 2014, 2016). These studies show that about 50% of the xylan residues in *Arabidopsis* are acetylated with every even residue bearing acetylation at the O-2 or O-3 position or both (Xiong et al. 2015; Busse-Wicher et al. 2016). These systems also possess MeGlcA at every 8th residue(Brown et al. 2007). However, it is unclear if these MeGlcA residues also maintain a periodic pattern like the acetyl groups. The acetylation pattern in *Arabidopsis* also plays an important role in modulating cellulose fibril coalescence as revealed from scanning electron microscope (SEM) and atomic force microscope (AFM) studies that show disruption in cellulose organization on minor mutations in the xylan backbone (Crowe et al. 2021).

As acetylation is usually lost in harsh experimental conditions, MD simulations act as a useful tool to obtain a microscopic understanding of the key interactions involved in plant cell wall organization. MD simulations of docked xylan show stable twofold helical screw conformations of xylan on both hydrophobic and hydrophilic cellulose surfaces (Busse-Wicher et al. 2014). However, strong binding of xylan to the hydrophilic surface was feasible only when the xylan was periodically acetylated and oriented in twofold helical screw (Busse-Wicher et al. 2014). In contrast to hardwood xylans, softwood xylans or mannans in spruce do not have a periodic acetylation pattern, thereby preventing the tight association with cellulose surfaces (Martínez-abad and Jiménez-quero 2020) although even spacing for MeGlcA and Ara residues in softwood xylans has been reported (Busse-Wicher et al. 2016; Martínez-Abad et al. 2017). Thus, it is evident that ordered patterns of acetyl substitution have a key role in stabilizing interactions with cellulose surface and are highly correlated with the extractability and recalcitrance of lignocellulosic biomass (Martínez-abad et al. 2018). Thus, a more detailed study is required to outline how the presence of a periodic pattern of Ac substitutions in xylan influences its interactions with cellulose.

The position of substitution has also been observed to play a central role in dictating different orientations of the xylan backbone with cellulose or lignin. Acetylation at the O-2 position in mannans has been shown to impart conformational rigidity with cellulose-like conformations in comparison to more flexible O-3 substituted conformations (Berglund et al. 2020). Similarly, our previous study using unrestrained MD simulations revealed that the presence of Ac groups at O-2 position favours twofold helical screw conformations of xylan that interact effectively with the (110) hydrophilic surface of cellulose, while O-3 acetylated xylan maintains a threefold helical screw conformation probably permitting to interact with lignin (Gupta et al. 2021). The twofold helical screw conformations are primarily stabilized by specific interactions between X-O4 of xylan and C-O6 of cellulose. Thus, regioselectivity of acetylation also plays a key role in mediating interactions with the cellulose surface.

In this work, we examine the role of the position of substitution at the O2 and O3 positions in xylan in influencing interactions with the (100) hydrophobic surface by constructing models of periodically O-2 acetylated and O3-acetylated xylans. We compare these models with bare xylan and a xylan backbone with one MeGlcA substitution. Our results reveal that 2AcX conformations interact effectively with

the (100) hydrophobic surface in stable twofold helical screw conformations. These conformations are primarily stabilized by the formation of many hydrophobic contacts between the xylan and the cellulose surface. In addition, both xylan-xylan as well as xylan-cellulose hydrogen bonds impart rigidity to the twofold helical screw conformations of 2AcX. In contrast, 3AcX conformations maintain flexible threefold helical screw conformations on the hydrophobic cellulose surface. These results are similar to our previous study on the (110) hydrophilic surface that showed stable twofold helical screw conformations of 2AcX, while 3AcX maintained threefold helical screw conformation (Gupta et al. 2021). However, the tendency to form twofold helical screw conformations of 2AcX is much higher on the (100) hydrophobic face than on the (110) hydrophilic cellulose surface.

As periodically O-2 acetylated xylan (2AcX) interacts more effectively with the cellulose surface compared to 3AcX, two more xylan models were examined to understand the role of the degree of acetylation in dictating the orientation of the xylan backbone on the cellulose surface. The first one was a fully acetylated xylan model (2AcXA) and another one had single substitution by an Ac group (2AcXS). Our studies show desorption of 2AcXA from the (100) hydrophobic surface implying the existence of an optimum fraction of unsubstituted residues in the xylan backbone for interaction with the cellulose surface. 2AcXS shows a higher preference for the (100) hydrophobic surface than bare xylan but the number of substitutions in 2AcXS is not enough to stabilize the twofold helical screw conformations. Moreover, we observe that the twofold helical screw conformations are stabilized on the surface when the unsubstituted residues form ~ 20% more contacts than the substituted residues. Previous studies of xylan in contact with hydrophilic (010), (110) or hydrophobic surfaces the (100), (200) were either partially restrained or were directly docked to the cellulose in a twofold helical screw or employed a different force field and thus, cannot be directly correlated with the spontaneous changes observed in this work. A comparison of the results obtained in this work on the (100) hydrophobic cellulose surface with our previous work on (110) hydrophilic surface (Gupta et al. 2021) using unrestrained simulations elucidates the role of surface topology in stabilizing twofold helical screw conformations of 2AcX.

Methods

Models To be consistent with our previous work (Gupta et al. 2021), we constructed models for O-2 and O-3 acetylated xylan with the degree of polymerization DP = 11, denoted as 2AcX and 3AcX, respectively. As per the experimental data (Brown et al. 2007; Bromley et al. 2013; Busse-Wicher et al. 2014, 2016), the alternate residues on the xylan backbone (residues 2, 4, 6, and 10) were substituted with Ac groups and the 8th residue was substituted with a MeGlcA group. In addition to these models, two more models for α-1,2 were constructed (2AcXA and 2AcXS). In 2AcXA, all the residues of the xylan backbone were acetylated (residues 1–7, 9–11). In 2AcXS, one of the residues of the xylan backbone was acetylated (residue 4). In both these models, the MeGlcA residue was maintained intact at the 8th position. It may be noted that the single substitution in 2AcXS was performed at position 4 to avoid the flexibility issues observed for outer residues and to maintain periodic substitution with a uniform spacing of 4 residues between the Ac and MeGlcA substituted residue. For comparison, a xylan backbone with only one substitution by the MeGlcA group at the 8th residue was modelled, denoted as MeGlcAX. In addition, a model of bare xylan with no substitutions at all was also constructed, denoted as UnX. Figure 1 shows a representative snapshot of all the six xylan models that are simulated in this work.

CHARMM-GUI was used to construct the initial models of UnX, MeGlcAX, 2AcX, 2AcXS, 2AcXA, and 3AcX (Jo et al. 2011; Park et al. 2019). The cellulose microfibril was modeled as half of a hexagonal 36-chain elementary fibril that was obtained using cellulose builder (Gomes and Skaf 2012) using the Iβ polymorph (Nishiyama et al. 2002) with DP = 20. All the 6 xylan models were placed on the (100) hydrophobic cellulose surface as per the crystalline arrangement. This surface was chosen as it has a stronger affinity for xylan than (1–10) hydrophilic surface (Larsson et al. 1999; Bergenstråhle et al. 2008). This initial orientation is one of many possible conformations of xylan on the cellulose surface and a full exploration of multiple interactions poses is beyond the scope of this work. Although cellulose and hemicellulose are large polymers, simulations of small model systems with DP = 2–14 in the past have proven to be significant in capturing important

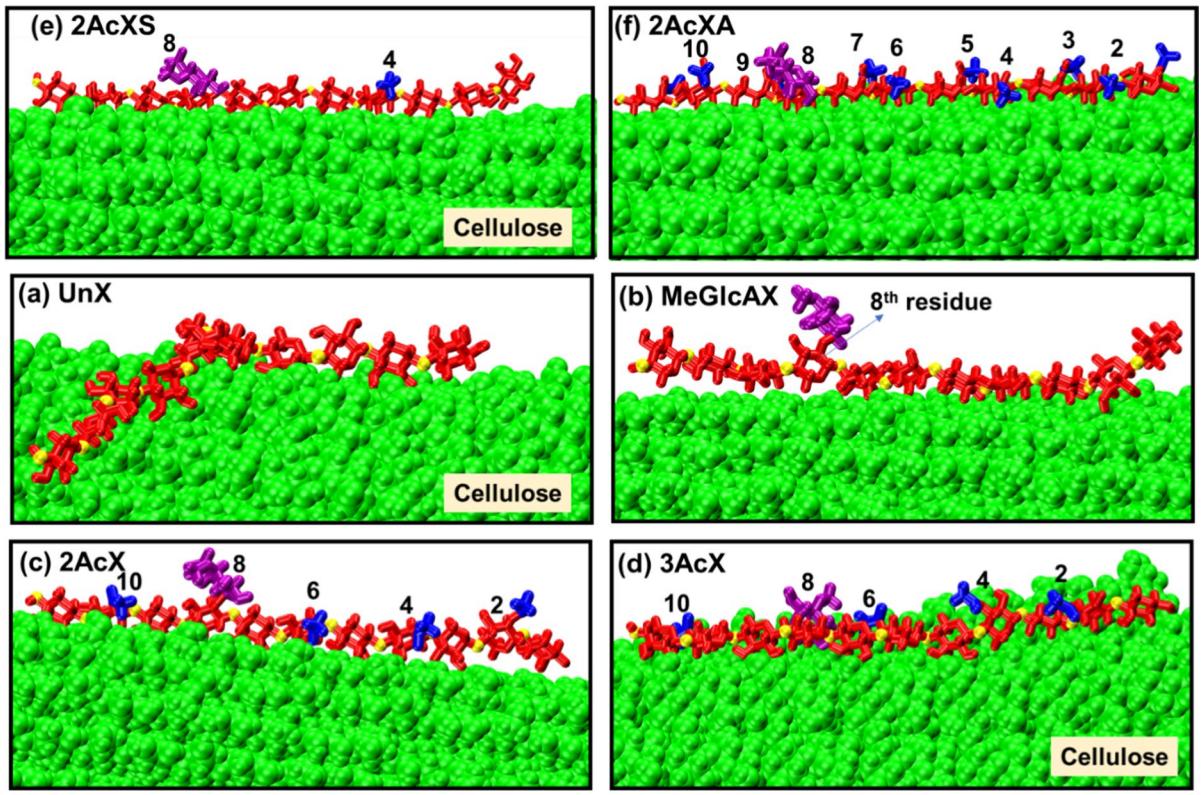

Fig. 1 Representative snapshots of **a** UnX, **b** MeGlcAX, **c** 2AcX, **d** 3AcX, **e** 2AcXS, and **f** 2AcXA on the (100) hydrophobic cellulose surface

microscopic details and thus have been used in this study as well (Berglund et al. 2016; Falcoz-Vigne et al. 2017; Grantham et al. 2017; Kong et al. 2022).

MD simulations The xylan-cellulose systems were solvated with TIP3P water (Jorgensen et al. 1983) and an ionic strength of 0.15 M was maintained using KCl. All-atom MD simulations were performed with GROMACS package (Abraham et al. 2015) and the CHARMM force field (Guvench et al. 2009) for carbohydrates was used for all the simulations. All the systems were first energy minimized followed by equilibration in the canonical NVT, and then isothermal-isobaric NPT ensembles for 4 ns each. Position restraints were applied to non-hydrogen atoms of the cellulose and xylan chains during the equilibration runs with a force constant of 1000 kcal mol^{-1} $Å^{-2}$. The v-Rescale thermostat with a time constant of 1 ps was used to maintain the temperature of 300 K during the simulations (Bussi et al. 2007). The Parrinello-Rahman barostat (Parrinello and Rahman 1981) was used to maintain a pressure of 1 bar in NPT simulations with a relaxation time of 2 ps and an isothermal compressibility of 4.5×10^{-5} bar^{-1}. The cut-off used for van der Waals interactions was 12 Å with a switch distance of 10 Å. The electrostatic interactions were treated with the Particle Mesh Ewald (PME) method (Darden et al. 1993). The LINCS algorithm was used to constrain all bond lengths involving hydrogen atoms (Hess et al. 1997; Hess 2008). The leapfrog algorithm as implemented in GROMACS was used to integrate the equations of motion using an integration time step of 2 fs for all the simulations. The data were dumped every 50 ps.

For all six xylan systems, sets of four independent simulations were performed. The initial configuration for each model was used to perform four sets of minimization and equilibration runs independently, followed by unrestrained production runs for 600 ns, starting from different velocity distributions (2400 ns cumulative for each system).

Analysis The terminal residues (1 and 11) were excluded from all the analyses. The presented data in

this work were averaged over four simulations for each of the systems. To calculate the root mean square deviations (RMSD) of the xylan backbone and the cellulose, an equilibrated structure was used as the reference structure. The RMSD and radius of gyration (R_g) were calculated using VMD (Humphrey et al. 1996) while GROMACS analysis tools were used to calculate the contacts and the hydrogen bond. A contact between any atom of the xylan and the cellulose surface is defined to be formed when the distance between these two atoms is ≤ 3.5 Å. The xylan conformations are designated as bound to the surface when each of the residues of the xylan backbone forms at least 15 contacts with the surface within a cut-off distance of 3.5 Å. The hydrogen bonds formed between the xylan models and the cellulose surface are defined using a geometric criterion (Luzar 2000; Torshin et al. 2002) with a donor–acceptor distance cut-off of 3.5 Å and the donor–acceptor angle cutoff of 30°. The standard error in all the computed quantities was calculated by averaging over time for each of the four simulations performed for each of the xylan models using the standard error formula ($E = \frac{\sigma}{\sqrt{N}}$, where $\sigma = \sqrt{x^2 - x^2}$ for any given observable x) in the gmx analyze tool of GROMACS.

Results and discussion

Xylan conformations

The cellulose fibers show a slight twist during simulations (Fernandes et al. 2011; Busse-Wicher et al. 2014; Pereira et al. 2017). However, the low RMSD of cellulose (~2.6–2.8 Å) for all the six models indicates that the cellulose fibers are stable (Table 1). The radius of gyration (R_g) of xylan for 2AcX on the (100) hydrophobic cellulose surface is higher than those for the UnX, MeGlcAX, 3AcX, 2AcXS, and 2AcXA models (Table 1). The root mean square deviations (RMSD) of all the models are comparable. R_g and RMSD for 2AcX show lower fluctuations than the other five models indicating formation of stable 2AcX conformations on the cellulose surface.

The local flexibility or rigidity of the xylan conformations can be characterized by measuring the dihedral angles at the β-(1,4) glycosidic linkage, ϕ = C4(i)-O4(i)-C1($i+1$)-O5($i+1$), and Ψ = C5(i)-C4(i)-O4(i)-C1($i+1$) between the ith and ($i+1$)th residues (Gupta et al. 2021). The sum of glycosidic dihedral angles can be used to characterize xylan conformations as twofold ($\phi + \Psi = 120°$) and threefold helical screw ($\phi + \Psi = 190°$) (Mazeau et al. 2005; French and Johnson 2009).

The histograms of ($\phi + \Psi$) for UnX on the (100) hydrophobic surface are centered around $\phi + \Psi = 190°$ (Fig. 2a–d, f, h) indicating that the UnX conformations are mostly threefold helical screw. However, the sum of ($\phi + \Psi$) around the inner residues (residues 6, 8) of UnX indicates occasional preference for the twofold helical screw conformation as reflected by an additional minor peak at $\phi + \Psi = 85$–$95°$ (Fig. 2e, g). It may be noted that only one out of four simulations for UnX shows any population of a twofold helical screw after 300 ns of simulation time. Thus, UnX conformations prefer to retain threefold helical screw conformations on the (100) hydrophobic cellulose surface. This is similar to previous MD simulations of bare xylan that adsorbed in the threefold helical screw conformation on the cellulose surface (Falcoz-Vigne et al. 2017; Gupta et al. 2021). However, these results contrast with another MD study using GLYCAM06 force field where bare xylan maintained twofold helical screw on (100) surface (Martínez-Abad et al. 2017). Thus, the use of different force fields may be responsible for the observed differences in the conformations of bare xylan (Martínez-Abad et al. 2017).

In the presence of a single MeGlcA substitution, the xylan prefers to form a twofold helical screw

Table 1 Average values of R_g, $RMSD_{xylan}$, $RMSD_{cell}$ for different models of xylan on the (100) hydrophobic cellulose surface

	UnX	MeGlcAX	2AcX	3AcX	2AcXS	2AcXA
R_g (Å)	12.9 (0.1)	13.4 (0.1)	14.0 (0)	13.3 (0.2)	13.2 (0.2)	13.4 (0.2)
$RMSD_{xylan}$ (Å)	3.3 (0.2)	2.8 (0.1)	3.4 (0)	3.6 (0.3)	3.2 (0.1)	4.0 (0.3)
$RMSD_{cellulose}$ (Å)	2.7 (0)	2.6 (0)	2.6 (0)	2.6 (0)	2.8 (0.3)	2.6 (0)

The presented data are averaged over four simulations for each model

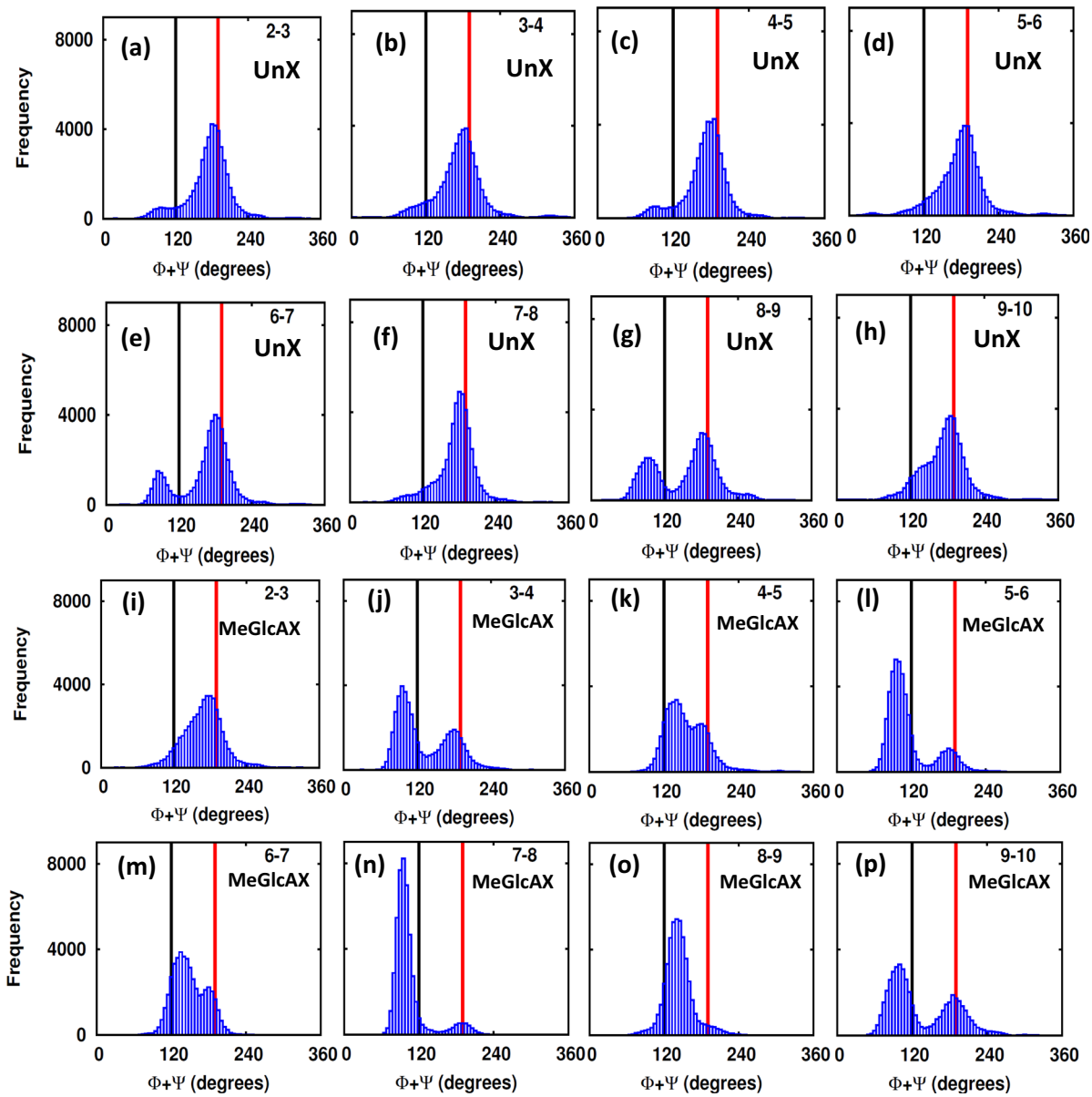

Fig. 2 Histograms for **a**–**h** UnX and **i**–**p** MeGlcAX conformations on the hydrophobic cellulose surface. The presented data are averaged over four simulations for each model

conformation on the hydrophobic surface. This is evident from the distributions of the $\phi+\Psi$ for MeGlcAX showing all residues except 2 and 8 with bimodal distributions with minor peaks around $\phi+\Psi=170$–$180°$ and major peak around $\phi+\Psi=85$–$130°$ (Fig. 2j–n, p). Residue 2 being farthest from the MeGlcA substituted residue 8 maintains a strictly threefold helical screw conformation, while the substituted 8th residue itself forms a twofold helical screw conformation (Fig. 2i, o). This indicates that a significant proportion of the MeGlcAX population forms twofold helices while a few maintain threefold helical screw. Surprisingly, the major peak is located around $\phi+\Psi=85$–$95°$ for residues 3, 5, 7 and 9 and around $\phi+\Psi=125$–$140°$ for residues 4, 6, and 8 of MeGlcAX (Fig. 2i–p). The population of twofold helical

screw conformations increases towards the MeGlcA substituted residue and attains a maximum at the MeGlcA substituted residue with a uniform histogram plot having a peak centered around $\phi+\Psi=130–140°$. This clearly reflects the effect of the presence of even a single MeGlcA substitution on surface where threefold helical conformations are dominant for MeGlcAX conformations and only the residues around the MeGlcA substituted residue showed a minor population in twofold helical screw (Gupta et al. 2021).

The role of periodic substitutions at O-2 position in dictating twofold helical screw conformations is revealed from the glycosidic dihedral angle distribution for 2AcX conformations. In 2AcX, all the residues except the one adjacent to the MeGlcA substituted residue strictly maintain twofold helical screw conformations as indicated by the unimodal distributions of $\phi+\Psi$ with a sharp peak around $\phi+\Psi=120°$ (Fig. 3a–h). In comparison to our previous study on the (110) hydrophilic cellulose surface, the percentage of population in twofold helical screw conformations is much higher on the (100) hydrophobic surface (Gupta et al. 2021). Previous 50 ns of MD simulation of docked xylan showed less stable conformations of periodically acetylated xylan as compared to bare xylan on the (100) hydrophobic cellulose surface, using interaction energies as a metric of stability (Busse-Wicher et al. 2014). Thus, the simulation time and the initial xylan orientation and use of restraints may play a role in dictating the xylan orientations on the cellulose surface in MD simulations.

The histograms for 3AcX clearly reveal the consistent preference of all the residues to maintain the threefold helical screw conformations with a sharp peak around $\phi+\Psi=175–185°$ (Fig. 3i-p). The substituted residues 2, 4, 6, and 8 show a minor peak centred around 100–110° but the majority of the population forms a threefold helical screw with a sharp peak centred around 190° (Fig. 3i, k, m, o). This behavior is consistent with the results obtained for 3AcX on the hydrophilic surface (Gupta et al. 2021). 3AcX conformations revert to threefold helical screw on the hydrophobic surface within 10–20 ns even if twofold helical screw conformations are formed occasionally.

2AcXS conformations show bimodal distributions for all the residues except 7 and 8, indicating formation of both twofold and threefold helical screw conformations (Fig. 4a–e, h). The MeGlcA substituted residue and the residue adjacent to it show twofold helical screw conformations as indicated by a peak around $\phi+\Psi=110–130°$ (Fig. 4f–g). Notably, the Ac substituted residues and the inner residue adjacent to the Ac substituted residues show almost equal populations for twofold and threefold helical screw (Fig. 4b, c). This indicates that the presence of one Ac substitution at O-2 position favors the formation of twofold helical screw conformation of xylan on the (100) hydrophobic cellulose surface as compared to bare xylan. However, the probability to form twofold helical screw conformations for 2AcXS is much lower than MeGlcAX. Thus, it may be suggested that the presence of single Ac group on the xylan backbone is not enough to form stable twofold helical screw conformations on the surface.

The fully acetylated xylan model, 2AcXA shows mostly threefold helical screw conformations for all the residues except a few inner residues around the MeGlcA residue that have a minor population in twofold helical screw (Fig. 4i–p). Previous studies show that higher number of unsubstituted residues on xylan backbone promote xylan-xylan interactions rather than xylan-cellulose interactions for bacterial cellulose (Kabel et al. 2007). Moreover, a more than 50% increase in the number of substituted residues on the xylan backbone such as ~ 70% Ac and 57% Ara decorations in xylan obstructed interactions with bacterial cellulose. This clearly demonstrates that the presence of an optimum number of unsubstituted residues on the xylan backbone as facilitated by periodic substitution for stabilizing twofold helical screw conformations on the cellulose surface along with the presence of substitutions at O2 position.

We also computed the percentage of conformations in twofold helical screw for each of the residues in the six xylan models on the (100) hydrophobic cellulose surface (Table 2) and compared them to our previous study on the (110) hydrophilic cellulose surface (Gupta et al. 2021) (Table 3). These calculations show that the inner residues of 2AcX have the highest preference to form twofold helical screw conformations on the hydrophobic surface (Table 2).

The MeGlcA substituted residue (residue 8) and the inner residue adjacent to it (residue 7) show higher percentages of twofold helical screw conformations for MeGlcAX and 2AcXS on the (100) hydrophobic surface than the other four models. UnX shows the lowest percentage of twofold helical screw conformations on both cellulose surfaces.

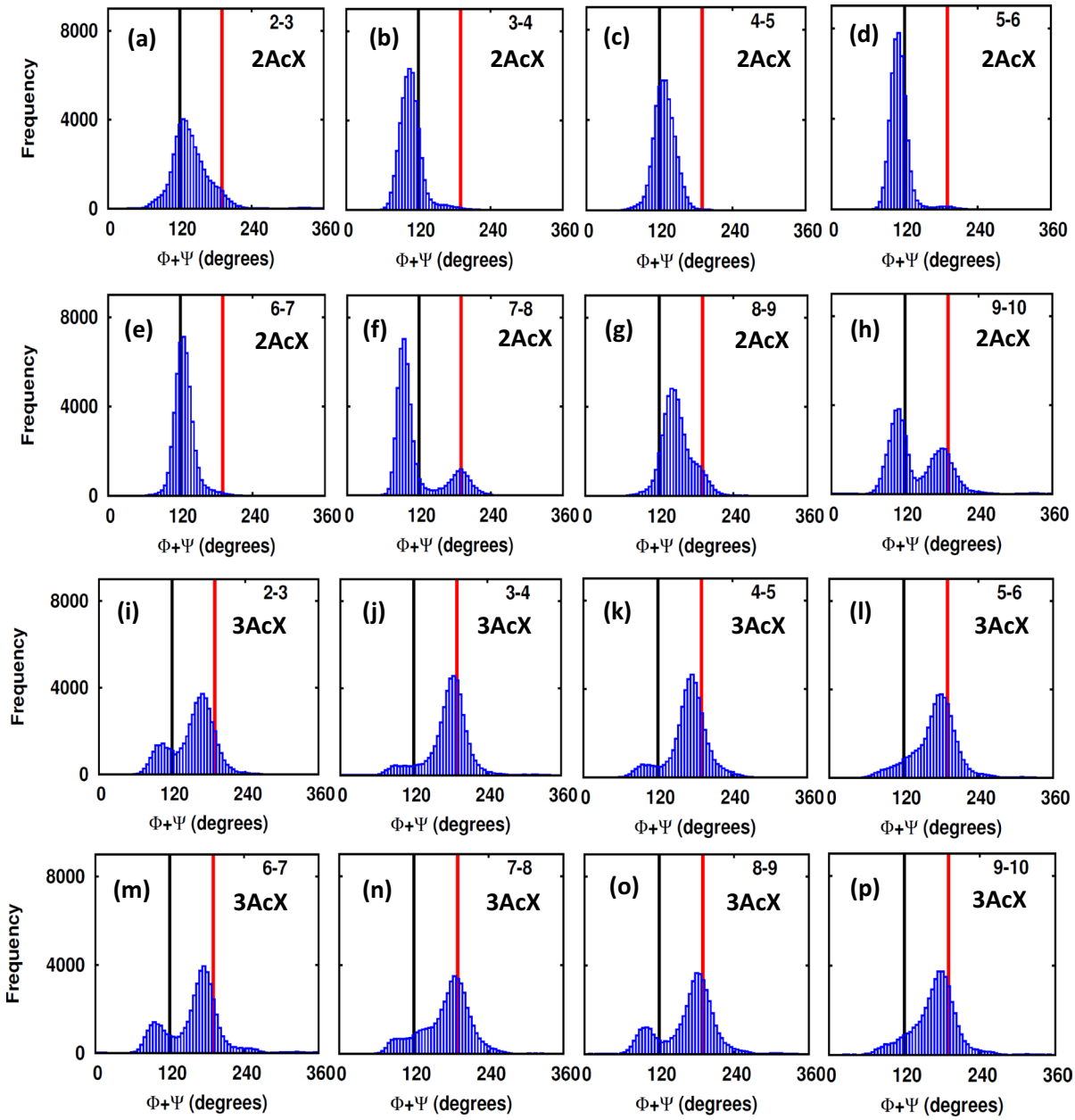

Fig. 3 Histograms for **a**–**h** 2AcX and **i**–**p** 3AcX conformations on the hydrophobic cellulose surface. The presented data are averaged over four simulations for each model

3AcX shows similar behavior on changing the cellulose surface from hydrophilic to hydrophobic. The hydrophobic surface shows a higher percentage of twofold helical screw conformations for all four models (UnX, MeGlcAX, 2AcX, and 3AcX) as compared to the hydrophilic surface. This clearly demonstrates that, irrespective of the substitution pattern, the twofold helical screw conformations are much more stable on the hydrophobic cellulose surface than the hydrophilic surface. Thus, it is of interest to determine the specific interactions that lead to varying stability of twofold xylan conformations on the cellulose surfaces.

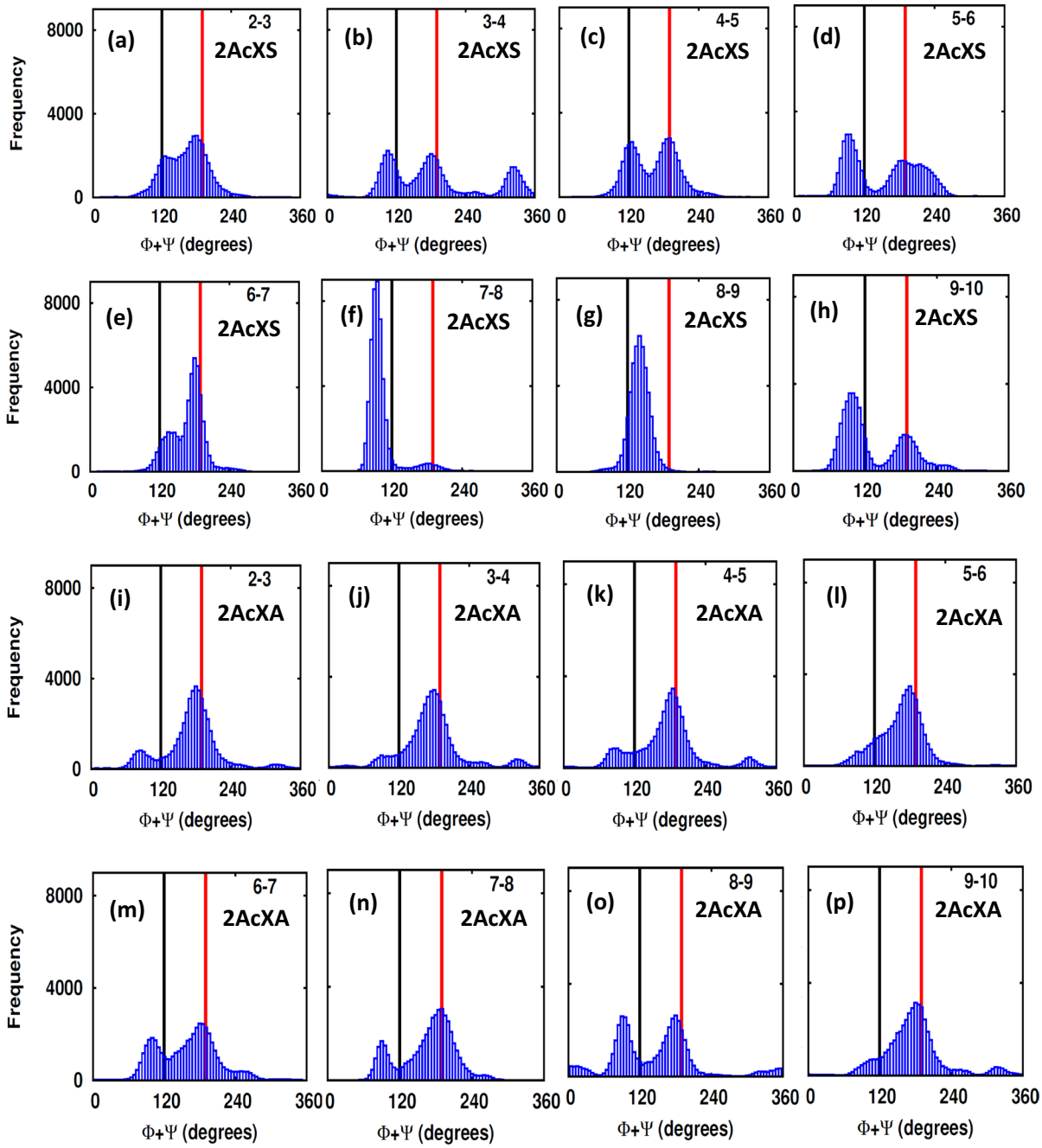

Fig. 4 Histograms for **a**–**h** 2AcXS and **i**–**p** 2AcXA conformations on the hydrophobic cellulose surface. The presented data are averaged over four simulations for each model

Intramolecular and intermolecular interactions

To obtain deeper insights into how 2AcX conformations form stable twofold helical screw conformations of xylan on the (100) hydrophobic cellulose surface, we calculated the number of intermolecular contacts, N_c, between xylan and the surface (Table 4). 2AcX forms the largest number of contacts followed by MeGlcAX. N_c is statistically similar for the UnX, 3AcX, and 2AcXA conformations.

Table 2 Percentage of conformations in twofold helical screw for various models on the (100) hydrophobic cellulose surface

Models	Residues							
	2	3	4	5	6	7	8	9
UnX	14.3 (1.0)	17.7 (2.4)	14.9 (2.0)	15.4 (6.3)	16.7 (4.6)	14.2 (5.1)	25.2 (9.0)	21.0 (9.4)
MeGlcAX	23.7 (3.1)	49.6 (8.5)	46.5 (8.9)	63.1 (9.8)	52.5 (1.6)	70.6 (6.0)	62.7 (5.7)	44.3 (2.7)
2AcX	64.7 (5.8)	85.2 (3.7)	85.4 (4.6)	94.3 (1.0)	91.0 (2.4)	61.9 (7.2)	52.6 (6.5)	53.4 (7.2)
3AcX	31.3 (2.1)	12.5 (2.9)	15.7 (1.4)	19.8 (9.4)	25.3 (8.1)	21.4 (10.4)	21.0 (8.6)	21.6 (5.7)
2AcXS	32.9 (8.1)	32.5 (19.5)	39.6 (21.7)	32.7 (18.3)	24.9 (16.6)	70.4 (5.0)	67.8 (4.4)	46.6 (1.9)
2AcXA	29.3 (17.1)	32.9 (18.0)	31.4 (16.9)	38.1 (18.1)	40.4 (14.9)	36.9 (15.8)	44.2 (15.9)	36.0 (19.1)

The presented data are averaged over four simulations for each model

Table 3 Percentage of conformations in twofold helical screw for various models on (110) hydrophilic cellulose surface

Models	Residues							
	2	3	4	5	6	7	8	9
UnX	10.8 (1.9)	14.1 (3.4)	14.3 (2.9)	11.8 (2.0)	12.7 (2.2)	15.9 (3.0)	14.6 (5.4)	12.7 (1.6)
MeGlcAX	11.8 (0.8)	11.4 (2.2)	12.8 (2.3)	13.5 (5.1)	6.9 (3.3)	10.5 (4.5)	18.5 (1.9)	14.1 (4.5)
2AcX	51.4 (9.7)	55.9 (10.6)	49.8 (10.2)	43.5 (13.3)	31.0 (10.9)	10.7 (5.1)	15.4 (5.0)	18.0 (1.8)
3AcX	25.1 (5.5)	22.8 (2.7)	20.4 (3.8)	11.8 (4.2)	17.6 (4.5)	13.6 (2.4)	17.6 (5.6)	14.3 (2.8)

The presented data are averaged over four simulations for each model

Table 4 Average values of order metrics for different xylan models (t > 400 ns) for different models of xylan on the (100) hydrophobic cellulose surface

	Type of residues	UnX	MeGlcAX	2AcX	3AcX	2AcXS	2AcXA
N_C	All	255 (17)	327 (19)	353 (3)	197 (3)	295 (28)	177 (64)
	Unsubstituted	24 (2)	40 (2)	42 (0)	25 (5)	30 (3)	NA
	per Ac			32 (1)	19 (3)	26 (5)	17 (7)
	MeGlcA		49 (1)	58 (1)	21 (6)	59 (2)	40 (16)
% bound ($N_C < 15$)		84.1 (4.5)	92.6 (2.6)	96.0 (0.8)	85.8 (7.5)	83.6 (7)	60.1 (10)
N_{HB}	All	6 (0)	9 (1)	9 (0)	5 (1)	8 (1)	4 (2)
	Unsubstituted	6(0)	8(1)	8 (1)	3 (1)	7 (1)	NA
	Ac	NA	NA	0 (0)	0 (0)	0 (0)	3 (1)
	MeGlcA	NA	1(0)	1(0)	1(0)	1 (0)	1(0)
Intra-molecular H bonding		1 (0)	3 (0)	3 (0)	1 (0)	2 (0)	2 (0)

The presented data are averaged over four simulations for each model

Categorizing the N_c into individual contributions from substituted and unsubstituted residues (Table 2) reveals the role of these residues in sustaining stable twofold helical screw conformations (Table 4). Firstly, the number of contacts formed by Ac substituted, MeGlcA substituted, and unsubstituted residues for 2AcX is larger than all other xylan models. A visual inspection of the simulations also confirms that Ac substitutions for 2AcX orient towards the surface, unlike 3AcX. Secondly, although the unsubstituted residues of both MeGlcAX and 2AcX form a comparable number of contacts with the hydrophobic surface, the Ac substituted residue of 2AcX forms 20% fewer contacts

(≈32) than the unsubstituted residues (≈42) of both 2AcX and MeGlcAX. Interestingly, the acetylated residues in 3AcX and 2AcXA form a similar number of contacts (≈17) revealing that the presence of substitutions at the O3 position and substituting all the O2 positions in xylan has a similar effect on xylan-cellulose interactions.

These observations again suggest the presence of an optimum number of unsubstituted residues for the formation of stable twofold helical screw xylan conformations on the (100) hydrophobic cellulose surface. In our simulations, the ratio of the number of contacts formed by substituted residues to unsubstituted residues needed to sustain twofold helical screw xylan conformations on the surface was around 0.76. Above this ratio, threefold helical screw conformations of xylan are more favourable. This is further evident from our previous studies where the number of contacts formed by both the substituted and unsubstituted residues of 2AcX on the hydrophilic surface were comparable (~26–27)(Gupta et al. 2021) resulting in the formation of a much lower percentage of twofold helical screw conformations as compared to the hydrophobic cellulose surface (Table 2).

Visual inspection of the simulations shows that MeGlcA is always oriented away from the cellulose surface for MeGlcAX and 2AcX throughout the simulation. In two of the simulations for 3AcX, MeGlcAX interacts with the surface for ~100 ns before flipping away from the surface. Previous studies have also shown that MeGlcA has low affinity for the cellulose surface(Linder et al. 2003; Martínez-Abad et al. 2017).

Next, we investigate the role of hydrogen bonds in xylan-cellulose interactions. UnX, 3AcX, and 2AcXA form, on average, 5–6 hydrogen bonds with the hydrophobic surface (Table 4) whereas MeGlcAX, 2AcX, and 2AcXS form ≈9–this is much higher than 2AcXA due to the availability of more unsubstituted residues that can interact with the cellulose surface. In contrast to the hydrophilic surface, the acetylated oxygens (X-OX2) of 2AcX and 3AcX do not hydrogen bond with the hydrophobic surface. Akin to the hydrophilic cellulose surface, the MeGlcA substituted residue consistently forms one hydrogen bond with the hydrophobic cellulose surface for all the models(Gupta et al. 2021). Figure 5 also shows that majority of 2AcX, 2AcXS, and MeGlcAX conformations form 7–10 hydrogen bonds with the

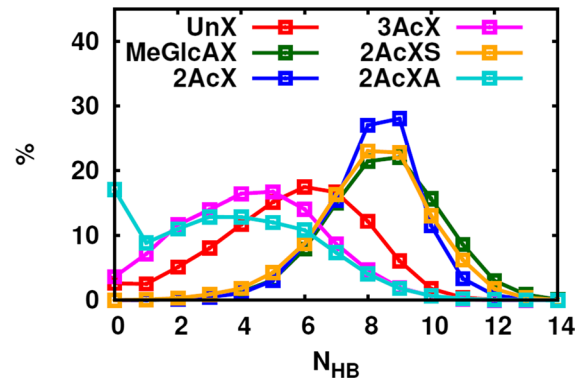

Fig. 5 Distribution of hydrogen bonds formed between various xylan systems and the hydrophobic cellulose surface. The presented data are averaged over four simulations for each model

hydrophobic surface, followed by UnX (4–7), 3AcX (3–6), and 2AcXA (1–6).

UnX and 3AcX form ≈1 intra-molecular hydrogen bond, while 2AcXA and 2AcXS form ≈2. In contrast, 2AcX and MeGlcAX conformations are stabilized by ≈3 intra-molecular hydrogen bonds. Focusing on the xylan models adopting a twofold screw, in 2AcX and 2AcXS, oxygen X-O5 acts as an acceptor. X-O2 also occasionally acts as acceptor in 2AcXS. The cellulose structure is also stabilized by the presence of intramolecular hydrogen bonds between C-O3 and C-O5(Nishiyama et al. 2002) and such bonding is expected to stabilize twofold helical screw xylan conformations as well(Pereira et al. 2017).

96% of 2AcX conformations remain bound to the cellulose surface, followed by MeGlcAX ≈93% (Table 4). The fraction of xylosyl residues bound to the cellulose surface is statistically similar for UnX, 3AcX, and 2AcXS models. However, UnX and 3AcX do not show detachment from the hydrophobic surface unlike the hydrophilic surface(Gupta et al. 2021). 2AcXA has the least number of bound xylan conformations (~60%) as compared to all other models implying an optimum number of unsubstituted residues needed to interact with the cellulose surface effectively. The visual inspection shows partial (Fig. 6a) and complete (Fig. 6b) desorption of the xylan from the surface for two of the 2AcXA simulations. Despite the high percentage of bound conformations for various models, only 2AcX shows the highest population of twofold helical screw xylan conformations for all the residues (Table 3). We

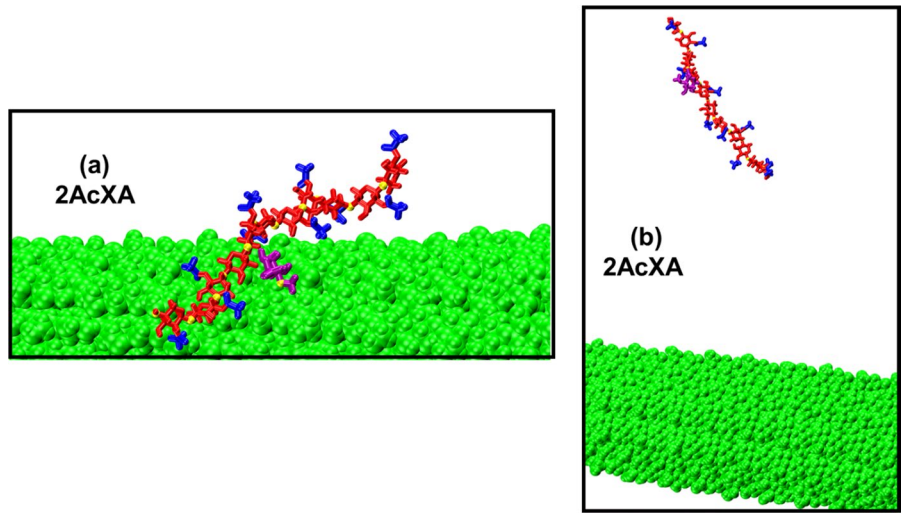

Fig. 6 2AcXA desorbed from the (100) hydrophobic cellulose surface

speculate that this is primarily because of the difference in the specific interactions between the xylan backbone and the cellulose surface for 2AcX and MeGlcAX.

Examining the specific interactions that stabilize xylan conformations on the hydrophobic surface reveals that the X-O2 (Fig. 7a) and X-O3 (Fig. 7b) of the unsubstituted residues of 2AcX interacts with C-O6, but the latter interactions are absent for MeGlcAX. X-O4 of the glycosidic bond of the substituted residues in 2AcX interacts with C-O6 (Fig. 7c). In addition, X-O4 of residues 2,4,6,8 of MeGlcAX and 2AcX interacts with C-O2 and C-O3. The other atom involved in the formation of glycosidic dihedral angle, X-O5 interacts with C-O6, C-O2 and C-O3 for residues 4, 6 and 8 in while residues 3, 5, 7 and 9 interact with C-O2 and C-O4 for MeGlcAX and 2AcX. OX2 of inner residues of 2AcX interacts with C-O5, C-O4, C-O3 (Fig. 7d-e), while OX3 of 3AcX has no preferable interactions with the cellulose surface. Interestingly, none of the OX2 residues for both 2AcXS and 2AcXA orient towards the surface. 2AcX are further stabilized by interactions between X-O3 of unsubstituted residues and C-O5. The loss of such interactions resulted in flexibility in xylan conformations (Pereira et al. 2017).

The specific interactions that stabilize the twofold helical screw conformations of 2AcX on the hydrophobic surface are the interactions of X-O3 of unsubstituted residues and X-OX2 of substituted residues with C-O6. These interactions are absent in the other five models. Solid state NMR and FT-IR experiments reveal that xylan migrates to the hydrophobic face from the hydrophilic face on pretreatment to promote aggregation of cellulose via the hydrophilic face (Liitiä et al. 2003; Penttilä et al. 2013). Previous studies also confirm the paramount role played by O6 of cellulose in stabilizing docked twofold helical screw conformations of xylan on the (010) or (020) hydrophilic cellulose surfaces (Busse-Wicher et al. 2014). Thus, hydrophobic contacts between xylan and cellulose dominate over hydrogen bonds to stabilize the twofold helical screw conformations of O-2 acetylated xylan on the hydrophobic cellulose surface. In contrast, the glucosidic rings are not fully exposed to facilitate hydrophobic stacking interactions on the hydrophilic surface so the electrostatic interactions supported by hydrogen bonding between the hydroxyl groups of xylan and the cellulose surface primarily stabilize the twofold helical screw conformation.

Conclusions

In this work, we have performed unrestrained MD simulations to understand the role of the acetyl substitutions at O-2 and O-3 positions of the xylan backbone in dictating the formation of twofold and threefold helical screw xylan conformations on the (100) hydrophobic cellulose surface. This study also investigates the effect of the degree of acetylation in influencing the twofold helical screw xylan conformations on the surface. Our results reveal that 2AcX conformations strictly maintain twofold helical screw

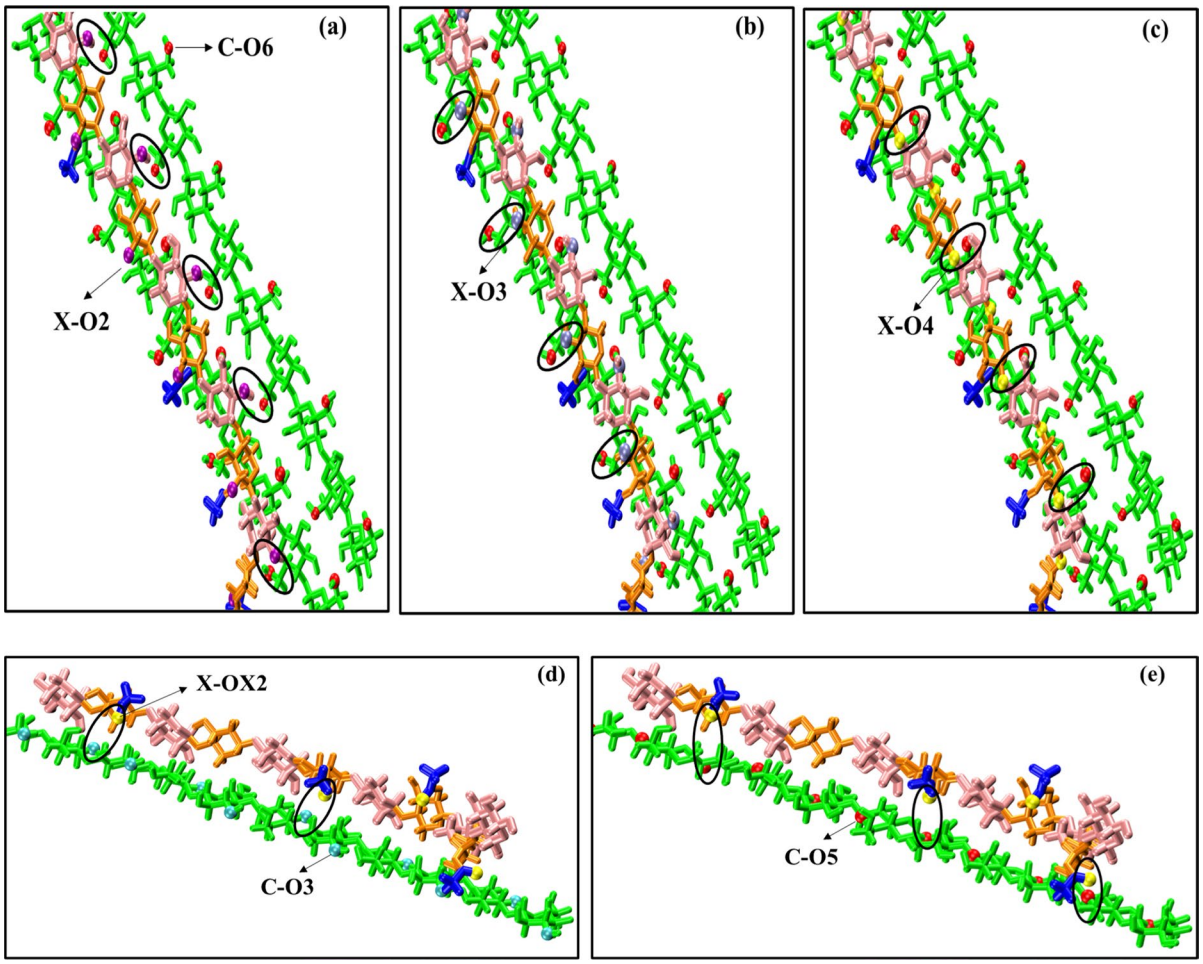

Fig. 7 Representative snapshots of specific interactions between 2AcX and hydrophobic cellulose surface. The substituted residues of 2AcX are shown in orange, while unsubstituted residues are shown in pink. The Ac substitutions are represented in blue and the cellulose surface is represented in green. X-O2, X-O3, X-O4, and C-O6 are shown in purple, ice-blue, yellow, and red, respectively for (**a**–**c**). X-OX2, C-O3 and C-O5 are shown in yellow, cyan, and red, respectively for (**d**, **e**). MeGlcA residue and waters are not shown for clarity

conformations on the hydrophobic surface with only a minor population of threefold helical screw for the residues adjacent to the MeGlcA residue. In contrast, UnX and 3AcX conformations maintain threefold helical screw on the hydrophobic surface. These observations are similar to our previous results with the (110) hydrophilic cellulose surface except that the percentage of 2AcX conformations in twofold helical screw is much higher for the hydrophobic surface. In addition, all the xylan models show much higher population of twofold helical screw conformations on the hydrophobic compared to the hydrophilic surface. MeGlcAX maintains mostly twofold helical screw conformations on the hydrophobic surface, although this percentage is much less than in 2AcX. Interestingly, the number of MeGlcAX conformations in twofold helical screw decreases with an increase in distance from the MeGlcA substituted residue. Thus, the presence of a single substitution on the xylan backbone is likely to trigger the formation of twofold helical screw conformations around the substituted residue on the hydrophobic cellulose surface. There have been previous reports explaining the importance of alternate substitutions for binding with the hydrophilic face but this may not be essential for binding to the hydrophobic face (Grantham et al. 2017).

Additional simulations of models substituted by Ac residue at one (2AcXS) and all positions (2AcXA) indicate the existence of an optimum fraction of substituted and unsubstituted residues to form stable twofold helical screw xylan conformations on the hydrophobic cellulose surface. 2AcXS shows a comparable probability for both twofold and threefold helical screw around the Ac substituted residue (residue 4) with MeGlcA substituted residue in twofold helical screw conformation. In contrast, 2AcXA maintains mostly threefold helical screw conformations.

A detailed analysis of 2AcX on the hydrophobic cellulose surface shows that twofold helical screw conformations are stabilized by the formation of many atomic contacts via both substituted and unsubstituted residues, in addition to intermolecular hydrogen bonds formed. 2AcX conformations are further stabilized by the formation of 3 intramolecular hydrogen bonds where O3 acts as a donor and O2/O5/X-O2 acts as acceptor. In 3AcX, the O3 position is occupied for substituted residues and is thus unavailable for hydrogen bonding or contacts resulting in the formation of threefold helical screw conformations. Moreover, none of the acetylated oxygens for 3AcX participate in either intra or intermolecular hydrogen bonding with the hydrophobic cellulose surface. It may be noted here that hydrogen bonding cannot be considered as the sole cause for the conformational preferences of xylan, rather formation of specific atomic contacts mediate the stability of twofold xylan conformations. Importantly, our studies reveal that to maintain stable twofold helical screw conformations of xylan on the hydrophobic surface, the number of contacts formed by unsubstituted residues should be about 20% higher than the substituted residues. The desorption of fully acetylated xylan from the cellulose surface clearly reflects that the presence of unsubstituted residues on the xylan backbone is vital for xylan-cellulose interaction. The key interactions that stabilize twofold helical screw conformations of 2AcX on the hydrophobic surface are formed between X-OX2:C-O6, X-O4:C-O6, X-O3:C-O5, and X-O3:C-O6. Thus, C-O6 plays a central role in stabilizing twofold helical screw conformations of xylan on both the hydrophilic and hydrophobic cellulose surfaces.

This work provides fundamental insights into the contribution of different interactions in the supramolecular organization of lignocellulosic biomass. Such advances in understanding such interactions may illuminate the development of improved methods to improve the conversion of biomass into sustainable products.

Acknowledgments This study was supported by SERB-POWER grant received from Science and Engineering Research Board (SERB), under the Department of Science and Technology (DST) Government of India (Reference No. SPG/2021/002224). This research was supported by the Center for Lignocellulose Structure and Formation, an Energy Frontier Research Center funded by the U.S. Department of Energy, Office of Science, Basic Energy Sciences under Award DE-SC0001090 and by the Genomic Science Program, Office of Biological and Environmental Research, U. S. Department of Energy (DOE) under Contract FWP ERKP752. This research used resources of the National Energy Research Scientific Computing Center, supported under Contract No. DE-AC02-05CH11231. Oak Ridge National Laboratory, which is supported by the Office of Science of the U.S. Department of Energy under Contract No. DE-AC05-00OR22725. This work used resources of the Compute and Data Environment for Science (CADES) at ORNL.

Author contributions MG performed all the simulations and analysis and wrote the main manuscript along with preparation of figures and tables. PD, LP and JS provided important inputs to improve the manuscript and reviewed the manuscript.

Funding Not applicable.

Data availability Not applicable.

Declarations

Conflict of interest There are no conflicts to declare.

Ethical approval and consent to participate Not applicable.

Consent for publication The authors give their consent for publishing the manuscript after peer review and its acceptance.

References

Abraham MJ, Murtola T, Schulz R et al (2015) Gromacs: high performance molecular simulations through multi-level parallelism from laptops to supercomputers. SoftwareX 1–2:19–25. https://doi.org/10.1016/j.softx.2015.06.001

Bergenstråhle M, Wohlert J, Larsson PT et al (2008) Dynamics of cellulose−water interfaces: NMR spin−lattice relaxation times calculated from atomistic computer simulations. J Phys Chem B 112:2590–2595

Berglund J, Angles d'Ortoli T, Vilaplana F et al (2016) A molecular dynamics study of the effect of glycosidic linkage type in the hemicellulose backbone on the molecular chain flexibility. Plant J 88:56–70. https://doi.org/10.1111/tpj.13259

Berglund J, Kishani S, Morais de Carvalho D et al (2020) Acetylation and sugar composition influence the (in)solubility of plant β-mannans and their interaction with cellulose surfaces. ACS Sustain Chem Eng 8:10027–10040. https://doi.org/10.1021/acssuschemeng.0c01716

Bootten TJ, Harris PJ, Melton LD, Newman RH (2004) Solid-state 13C-NMR spectroscopy shows that the xyloglucans in the primary cell walls of mung bean (*Vigna radiata* L.) occur in different domains: a new model for xyloglucan-cellulose interactions in the cell wall. J Exp Bot 55:571–583. https://doi.org/10.1093/jxb/erh065

Bosmans TJ, Stépán AM, Toriz G et al (2014) Assembly of debranched xylan from solution and on nanocellulosic surfaces. Biomacromol 15:924–930. https://doi.org/10.1021/bm4017868

Bromley JR, Busse-Wicher M, Tryfona T et al (2013) GUX1 and GUX2 glucuronyltransferases decorate distinct domains of glucuronoxylan with different substitution patterns. Plant J 74:423–434. https://doi.org/10.1111/tpj.12135

Brown DM, Goubet F, Wong VW et al (2007) Comparison of five xylan synthesis mutants reveals new insight into the mechanisms of xylan synthesis. Plant J 52:1154–1168. https://doi.org/10.1111/j.1365-313X.2007.03307.x

Busse-Wicher M, Gomes TCF, Tryfona T et al (2014) The pattern of xylan acetylation suggests xylan may interact with cellulose microfibrils as a twofold helical screw in the secondary plant cell wall of *Arabidopsis thaliana*. Plant J 79:492–506. https://doi.org/10.1111/tpj.12575

Busse-Wicher M, Li A, Silveira RL et al (2016) Evolution of xylan substitution patterns in gymnosperms and angiosperms: implications for xylan interaction with cellulose. Plant Physiol 171:2418–2431. https://doi.org/10.1104/pp.16.00539

Bussi G, Donadio D, Parrinello M (2007) Canonical sampling through velocity rescaling. J Chem Phys 126:014101. https://doi.org/10.1063/1.2408420

Celińska E, Nicaud JM, Białas W (2021) Hydrolytic secretome engineering in *Yarrowia lipolytica* for consolidated bioprocessing on polysaccharide resources: review on starch, cellulose, xylan, and inulin. Appl Microbiol Technol 105:975–989. https://doi.org/10.1007/s00253-021-11097-1

Chundawat SPS, Beckham GT, Himmel ME, Dale BE (2011) Deconstruction of lignocellulosic biomass to fuels and chemicals. Annu Rev Chem Biomol Eng 2:121–145. https://doi.org/10.1146/annurev-chembioeng-061010-114205

Cosgrove D (2014) Re-constructing our models of cellulose and primary cell wall assembly. Curr Opin Plant Biol 22:122–131

Cosgrove DJ, Jarvis MC (2012) Comparative structure and biomechanics of plant primary and secondary cell walls. Front Plant Sci 3:1–6. https://doi.org/10.3389/fpls.2012.00204

Crowe JD, Hao P, Pattathil S et al (2021) Xylan is critical for proper bundling and alignment of cellulose microfibrils in plant secondary cell walls. Front Plant Sci 12:1–19. https://doi.org/10.3389/fpls.2021.737690

Darden T, York D, Pedersen L (1993) Particle mesh Ewald: an N·log(N) method for Ewald sums in large systems. J Chem Phys 98:10089–10092. https://doi.org/10.1063/1.464397

de Carvalho DM, Berglund J, Marchand C et al (2019) Improving the thermal stability of different types of xylan by acetylation. Carbohydr Polym 220:132–140. https://doi.org/10.1016/j.carbpol.2019.05.063

Ebringerova A, Heinze T (2000) Xylan and xylan derivatives–biopolymers with valuable properties, 1. Naturally occurring xylans structures, isolation procedures and properties. Macromol Rapid Commun 21:869–883. https://doi.org/10.1002/1521-3927

Falcoz-Vigne L, Ogawa Y, Molina-Boisseau S et al (2017) Quantification of a tightly adsorbed monolayer of xylan on cellulose surface. Cellulose 24:3725–3739. https://doi.org/10.1007/s10570-017-1401-z

Fernandes AN, Thomas LH, Altaner CM et al (2011) Nanostructure of cellulose microfibrils in spruce wood. Proc Nat Acad Sci USA 108:E1195–E1203. https://doi.org/10.1073/pnas.1108942108

French AD, Johnson GP (2009) Cellulose and the twofold screw axis: modeling and experimental arguments. Cellulose 16:959–973. https://doi.org/10.1007/s10570-009-9347-4

Gomes TCF, Skaf MS (2012) Cellulose-builder: a toolkit for building crystalline structures of cellulose. J Comput Chem 33:1338–1346. https://doi.org/10.1002/jcc.22959

Grantham NJ, Wurman-Rodrich J, Terrett OM et al (2017) An even pattern of xylan substitution is critical for interaction with cellulose in plant cell walls. Nat Plants 3:859–865. https://doi.org/10.1038/s41477-017-0030-8

Gupta M, Rawal TB, Dupree P et al (2021) Spontaneous rearrangement of acetylated xylan on hydrophilic cellulose surfaces. Cellulose 28:3327. https://doi.org/10.1007/s10570-021-03706-z

Guvench O, Hatcher E, Venable RM et al (2009) CHARMM additive all-atom force field for glycosidic linkages between hexopyranoses. J Chem Theory Comput 5:2353–2370. https://doi.org/10.1021/ct900242e

Hess B (2008) P-LINCS: a parallel linear constraint solver for molecular simulation. J Chem Theory Comput 4:116–122. https://doi.org/10.1021/ct700200b

Hess B, Bekker H, Berendsen HJC, Fraaije JGEM (1997) LINCS: a linear constraint solver for molecular simulations. J Comput Chem 18:1463–1472. https://doi.org/10.1002/(SICI)1096-987X(199709)18:12%3c1463::AID-JCC4%3e3.0.CO;2-H

Humphrey W, Dalke A, Schulten K (1996) VMD: visual molecular dynamics. J Mol Graph 14:33–38. https://doi.org/10.1016/0263-7855(96)00018-5

Jo S, Song KC, Desaire H et al (2011) Glycan reader: Automated sugar identification and simulation preparation for carbohydrates and glycoproteins. J Comput Chem 32:3135–3141. https://doi.org/10.1002/jcc.21886

Johnson AM, Kim H, Ralph J, Mansfield SD (2017) Natural acetylation impacts carbohydrate recovery during deconstruction of *Populus trichocarpa* wood. Biotechnol Biofuels 10:1–12. https://doi.org/10.1186/s13068-017-0734-z

Jorgensen WL, Chandrasekhar J, Madura JD et al (1983) Comparison of simple potential functions for simulating liquid water Comparison of simple potential functions

for simulating liquid water. J Chem Phys 79:926. https://doi.org/10.1063/1.445869
Kabel MA, van den Borne H, Vincken JP et al (2007) Structural differences of xylans affect their interaction with cellulose. Carbohydr Polym 69:94–105. https://doi.org/10.1016/j.carbpol.2006.09.006
Kang X, Kirui A, Dickwella Widanage MC et al (2019) Lignin-polysaccharide interactions in plant secondary cell walls revealed by solid-state NMR. Nat Commun 10:347. https://doi.org/10.1038/s41467-018-08252-0
Köhnke T, Östlund Å, Brelid H (2011) Adsorption of arabinoxylan on cellulosic surfaces: influence of degree of substitution and substitution pattern on adsorption characteristics. Biomacromol 12:2633–2641. https://doi.org/10.1021/bm200437m
Kong Y, Li L, Fu S (2022) Insights from molecular dynamics simulations for interaction between cellulose microfibrils and hemicellulose. J Mater Chem A. https://doi.org/10.1039/d2ta03164g
Larsson PT, Hult EL, Wickholm K et al (1999) CP/MAS 13C-NMR spectroscopy applied to structure and interaction studies on cellulose I. Solid State Nucl Magn Reson 15:31–40. https://doi.org/10.1016/S0926-2040(99)00044-2
Liitiä T, Maunu SL, Hortling B et al (2003) Cellulose crystallinity and ordering of hemicelluloses in pine and birch pulps as revealed by solid-state NMR spectroscopic methods. Cellulose 10:307–316. https://doi.org/10.1023/A:1027302526861
Linder A, Bergman R, Bodin A, Gatenholm P (2003) Mechanism of assembly of xylan onto cellulose surfaces. Langmuir 19:5072–5077. https://doi.org/10.1021/la034355
Lindman B, Medronho B, Alves L et al (2021) Hydrophobic interactions control the self-assembly of DNA and cellulose. Q Rev Biophys 54:1–22. https://doi.org/10.1017/S0033583521000019
Ling Z, Edwards JV, Nam S et al (2020) Conformational analysis of xylobiose by DFT quantum mechanics. Cellulose 27:1207–1224. https://doi.org/10.1007/s10570-019-02874-3
Luzar A (2000) Resolving the hydrogen bond dynamics conundrum. J Chem Phys 113:10663–10675. https://doi.org/10.1063/1.1320826
Martínez-Abad A, Berglund J, Toriz G et al (2017) Regular motifs in xylan modulate molecular flexibility and interactions with cellulose surfaces. Plant Physiol 175:1579–1592. https://doi.org/10.1104/pp.17.01184
Martínez-abad A, Jiménez-quero A (2020) Influence of the molecular motifs of mannan and xylan populations on their recalcitrance and organization in spruce softwoods. Green Chem 22:3956–3970. https://doi.org/10.1039/d0gc01207f
Martínez-abad A, Giummarella N, Vilaplana F, Lawoko M (2018) Differences in extractability under subcritical water reveal interconnected hemicellulose and lignin recalcitrance in birch hardwoods. Green Chem 20:2534–2546. https://doi.org/10.1039/c8gc00385h
Mazeau K, Moine C, Krausz P, Gloaguen V (2005) Conformational analysis of xylan chains. Carbohydr Res 340:2752–2760. https://doi.org/10.1016/j.carres.2005.09.023
Nishiyama Y, Langan P, Chanzy H (2002) Crystal structure and hydrogen-bonding system in cellulose Iβ from synchrotron X-ray and neutron fiber diffraction. J Am Chem Soc 124:9074–9082. https://doi.org/10.1021/ja0257319
Park SJ, Lee J, Qi Y et al (2019) CHARMM-GUI Glycan Modeler for modeling and simulation of carbohydrates and glycoconjugates. Glycobiology 29:320–331. https://doi.org/10.1093/glycob/cwz003
Parrinello M, Rahman A (1981) Polymorphic transitions in single crystals: a new molecular dynamics method. J Appl Phys 52:7182–7190. https://doi.org/10.1063/1.328693
Pawar PMA, Koutaniemi S, Tenkanen M, Mellerowicz EJ (2013) Acetylation of woody lignocellulose: significance and regulation. Front Plant Sci 4:1–8. https://doi.org/10.3389/fpls.2013.00118
Penttilä PA, Várnai A, Pere J et al (2013) Xylan as limiting factor in enzymatic hydrolysis of nanocellulose. Bioresour Technol 129:135–141. https://doi.org/10.1016/j.biortech.2012.11.017
Pereira CS, Silveira RL, Dupree P, Skaf MS (2017) Effects of xylan side-chain substitutions on xylan-cellulose interactions and implications for thermal pretreatment of cellulosic biomass. Biomacromol 18:1311–1321. https://doi.org/10.1021/acs.biomac.7b00067
Scheller HV, Ulvskov P (2010) Hemicelluloses. Annu Rev Plant Biol 61:263–289. https://doi.org/10.1146/annurev-arplant-042809-112315
Simmons TJ, Mortimer JC, Bernardinelli OD et al (2016) Folding of xylan onto cellulose fibrils in plant cell walls revealed by solid-state NMR. Nat Commun 7:13902. https://doi.org/10.1038/ncomms13902
Teleman A, Tenkanen M, Jacobs A, Dahlman O (2002) Characterization of O-acetyl-(4-O-methylglucurono)xylan isolated from birch and beech. Carbohydr Res 337:373–377. https://doi.org/10.1016/S0008-6215(01)00327-5
Torshin IY, Weber IT, Harrison RW (2002) Geometric criteria of hydrogen bonds in proteins and identification of "bifurcated" hydrogen bonds. Protein Eng 15:359–363. https://doi.org/10.1093/protein/15.5.359
Tryfona T, Bourdon M, Delgado Marques R et al (2023) Grass xylan structural variation suggests functional specialization and distinctive interaction with cellulose and lignin. Plant J 113:1004–1020. https://doi.org/10.1111/tpj.16096
Wierzbicki MP, Maloney V, Mizrachi E, Myburg AA (2019) Xylan in the middle: understanding xylan biosynthesis and its metabolic dependencies toward improving wood fiber for industrial processing. Front Plant Sci 10:1–29. https://doi.org/10.3389/fpls.2019.00176
Wohlert M, Benselfelt T, Wågberg L et al (2022) Cellulose and the role of hydrogen bonds: not in charge of everything. Cellulose 29:1–23. https://doi.org/10.1007/s10570-021-04325-4
Xiong G, Dama M, Pauly M (2015) Glucuronic acid moieties on xylan are functionally equivalent to O-acetyl-substituents. Mol Plant 8:1119–1121. https://doi.org/10.1016/j.molp.2015.02.013
Zhao Z, Crespi VH, Kubicki JD et al (2014) Molecular dynamics simulation study of xyloglucan adsorption on cellulose surfaces: effects of surface hydrophobicity and side-chain variation. Cellulose 21:1025–1039. https://doi.org/10.1007/s10570-013-0041-1

Publisher's Note Springer Nature remains neutral with regard to jurisdictional claims in published maps and institutional affiliations.

Springer Nature or its licensor (e.g. a society or other partner) holds exclusive rights to this article under a publishing agreement with the author(s) or other rightsholder(s); author self-archiving of the accepted manuscript version of this article is solely governed by the terms of such publishing agreement and applicable law.